Electronic Research Archive

ERA, 31(8): 4968–4984.
DOI: 10.3934/era.2023254
Received: 07 April 2023
Revised: 15 May 2023
Accepted: 23 May 2023
Published: 13 July 2023

http://www.aimspress.com/journal/era

Research article

Numerical simulation analysis for the effect of water content on the intelligent compaction quality of roadbed

Yuan Ma[1], Yingcheng Luan[1,*], Shuangquan Jiang[2,3], Jianming Zhang[3] and Chuanle Wang[1]

[1] School of Transportation, Southeast University, Nanjing 211189, China
[2] School of Highway, Chang'an University, Xi'an 710064, China
[3] Sichuan Road and Bridge (Group) Co., Ltd., Chengdu 610041, China

*** Correspondence:** Email: luanyingcheng@seu.edu.cn; Tel: +8618366114315.

Abstract: In the process of intelligent compaction of roadbeds, the water content of the roadbed is one of the important influencing factors of compaction quality. In order to analyze the effect of water content on the compaction quality of roadbeds, this paper is developed by secondary development of Abaqus finite element numerical simulation software. At the same time, the artificial viscous boundary was set to eliminate the influence of boundary conditions on the results in the finite element modeling process, so that the numerical simulation can be refined to model. On this basis, the dynamic response analysis of the roadbed compaction process is performed on the finite element numerical simulation results. This paper established the correlation between compaction degree and intelligent compaction index CMV (Compaction Meter Value) and then analyzed the effect of water content on the compaction quality for the roadbed. The results of this paper show that the amplitude of the vertical acceleration is almost independent of the moisture content, and the vertical displacement mainly occurs in the static compaction stage. The vertical displacement changes sharply in the first 0.5 s when the vibrating wheel is in contact with the roadbed. The main stage of roadbed compaction quality increase is before the end of the first compaction. At the end of the first compaction, the roadbed compaction degree increased rapidly from 80% to 91.68%, 95.34% and 97.41%, respectively. With the increase in water content, the CMV gradually increased. At the end of the second compaction, CMV increased slightly compared with that at the end of the first compaction and stabilized at the end of the second compaction. The water content of the roadbed should be considered to be set slightly higher than the optimal water content of the roadbed by about 1% during the construction of the roadbed within the assumptions of this paper.

Keywords: road engineering; intelligent compaction; CMV; secondary development; water content

1. Introduction

Compaction is an important part of the roadbed construction process, which can significantly improve the strength, stiffness and stability of the roadbed [1]. However, the traditional compaction methods have limitations in the following aspects: 1) the roller parameters are usually set according to the operator's experience, and the compaction process has a large error; 2) the traditional compaction detection method usually conducts random checks on limited points, and cannot fully detect the uniformity of road compaction[2]; 3) the traditional compaction quality detection method is a lossy detection [3,4], which has a certain destruction; 4) the traditional compaction detection method cannot be real-time detection, belongs to the "result" detection, rather than "process" detection. Therefore, the traditional compaction and compaction quality evaluation method has the significant property of "manual interference (empirical) - point sampling (limitation) - pavement damage (destructive) - hindsight evaluation (lag)" [5].

Intelligent compaction technology is a hallmark of the development of modern compaction technology and one of the important revolutionary road engineering construction technologies that have emerged worldwide [6,7]. By integrating a high-precision positioning system, acceleration sensors, active compaction regulation and control system, on-board/background monitoring system, and other necessary sensing devices on the compactor, continuous dynamic monitoring of compaction quality and automatic optimization of compaction parameters are achieved to achieve optimal/target compaction quality [8,9]. Compared with traditional compaction technology, the transformative nature of intelligent compaction is not only reflected in the significant improvement of construction efficiency and quality by the use of information technology, but also in the intelligent scientific management mode that shifts the construction quality from after-the-fact inspection to after-the-fact control, and the digital transformation and upgrading of the construction process reconfigurable and data traceable [10,11].

Although intelligent compaction technology has been rapidly developed in recent years and widely used in many fields, the following problems still exist: 1) when establishing the intelligent compaction simulation model of the roadbed, the influence of the boundary conditions on the compaction results is ignored, which will lead to the deviation of the calculation results because of the influence of the boundary conditions; 2) when performing the numerical simulation of the intelligent compaction process of the roadbed, the soil parameters of the roadbed are not considered parameters change in real-time as compaction proceeds [12]. This will lead to a discrepancy between the numerical simulation model and the actual situation, which will inevitably bring limitations in the calculation results; 3) the current research on roadbed compaction does not consider the effect of water content on the final compaction results. This will lead to the conclusions obtained only for specific moisture content, making the generalizability of the research results insufficient.

In this paper, the problems of numerical simulation of intelligent compaction of roadbed are investigated. First, in order to eliminate the influence of boundary conditions on the calculation results in the numerical simulation modeling process, artificial viscous boundary is established. Further, to address the problem that the parameters of the roadbed cannot be changed in real time with the intelligent compaction process in the finite element numerical simulation, the finite element numerical simulation software is secondarily developed to realize refined modeling and obtain the intelligent

compaction dynamics response results. Then, the parameters corresponding to different roadbed soils are substituted into the numerical simulation model for calculation, and the corresponding kinetic responses of different roadbed soils are obtained respectively. Finally, based on the kinetic response of different water content of roadbed soils in the compaction process, the relationship between the corresponding compaction index and the intelligent compaction index CMV is established, respectively, and the influence of water content on the intelligent compaction index is analyzed, and the optimal construction water content is suggested. Then, the parameters corresponding to the different water content of roadbed soils are substituted into the numerical simulation model for calculation, and the corresponding kinetic responses of different roadbed soils are obtained respectively. Finally, based on the dynamic response of different water content of roadbed soils, the relationship between the corresponding compaction degree and CMV are established, respectively. The influence of water content on CMV is analyzed, and the optimal construction water content is suggested.

2. Methodology

In this paper, we eliminate the influence of boundary conditions on the calculation results in the modeling process of finite element numerical simulation by establishing an artificial viscous boundary. Then the secondary development of Abaqus finite element numerical simulation software is carried out to realize the dynamic changes of roadbed compaction process parameters and build a refined simulation model. The numerical simulation conditions of roadbed compaction with different water content are designed. The corresponding dynamic response results of the roadbed compaction process are obtained and analyzed. Then, the correlation between compaction degree and CMV is established, and the correlation between water content and CMV is analyzed.

2.1. Establishment of finite element numerical simulation model

2.1.1. Structure of roadbed

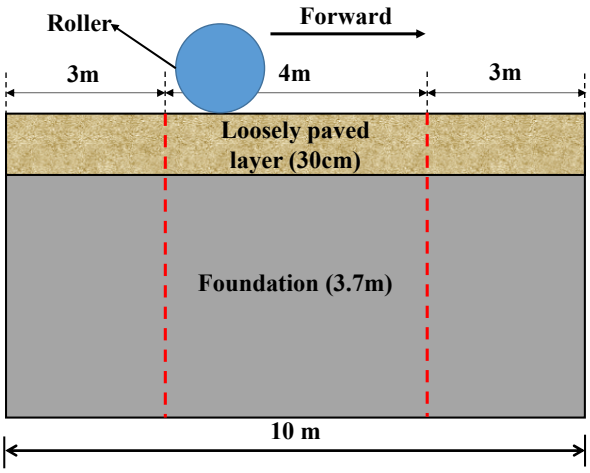

Figure 1. Roadbed structure.

The research results show that the influence range of the vibrating wheel in the horizontal

direction during compaction is about 3–5 m [13]. Therefore, when establishing the numerical simulation model, the horizontal direction is defined as 10 m, which can eliminate the influence brought by the size effect. In actual construction, the thickness of each layer of the roadbed loosened is 20–30 cm. Therefore, in this paper, the upper layer loosened thickness is defined as 30 cm, and the lower base is defined as 3.7 m. The schematic diagram of roadbed structure is shown in Figure 1.

2.1.2. Artificial boundary conditions

The purpose of setting artificial boundary is to avoid the reflection of vibration wave at the cut-off boundary of subgrade and simulate the properties of infinite domain, thus improving the accuracy of calculation area. At present, the typical method is to add damping on the boundary to absorb the wave energy [14]. For example, the infinite element boundary coming with ABAQUS makes use of this principle. However, this kind of boundary cannot resist static-dynamic unified load (gravity and excitation force), since pure damping has no resistance to static force, which leads to an overall settlement of the model. To this problem, Deeks et al. [15] proposed a viscoelastic artificial boundary for a plane strain model with springs attached on the boundary nodes as well as dampers (Figure 2). First, the spring is capable to modify the influence of amplitude attenuation caused by wave-front diffusion. On the other hand, it provides resilience to support static loads. Furthermore, to facilitate its implementation in the FE model, Dong et al. [16] proposed a method to use the modulus and damping of the peripheral boundary element to replace the springs and dampers on nodes. The modulus and damping (use Rayleigh damping proportional to stiffness) of the equivalent element can be calculated by Eq (1).

$$\begin{cases} \mathrm{E} = \alpha_N h \frac{G}{R} \\ \beta = \frac{\rho R}{2G}\left(\frac{c_S}{\alpha_T} + \frac{c_P}{\alpha_N}\right) \end{cases} \tag{1}$$

where: h is the thickness of equivalent element; G and ρ represent the shear modulus and material density respectively; R is the distance from the vibration source to the boundary; c_s and c_p represent the shear and dilatational wave velocity respectively; α_T and α_N are the correction coefficients, which were taken as 0.5 and 1.0.

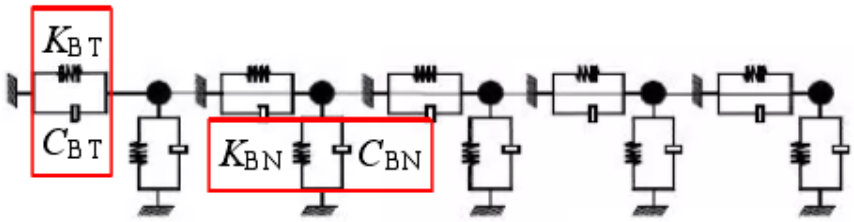

Figure 2. Principle of viscoelastic artificial boundary.

2.1.3. Roadbed structure and meshing

The vibration wave velocity during vibration compaction of the roadbed is calculated to be 150.9 m/s. The wavelength corresponding to the highest frequency can be calculated according to Eq (5). The wavelength of vibration wave during vibratory compaction is calculated to be λ = 4.31 m.

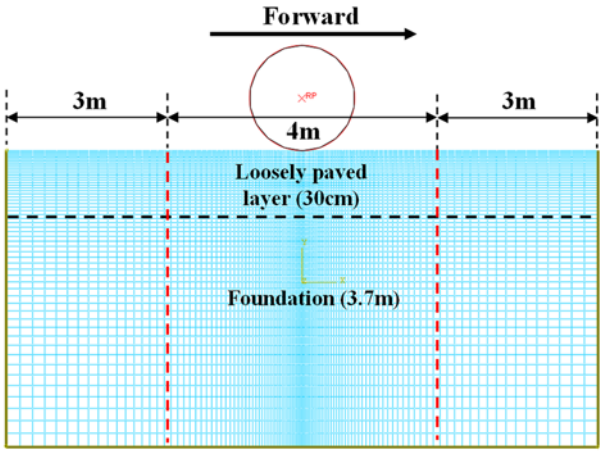

Figure 3. Finite element numerical simulation grid division diagram.

The selection of grid density is also an important aspect in numerical simulation. The selection of grid density should ensure both the accuracy of numerical simulation and sufficient computational efficiency. Related studies have shown [17] that the grid size is related to the computational accuracy, and to ensure the computational accuracy, the grid size needs to meet the requirements of Eq (2). Most of the excitation frequency of rollers in field tests is in the range of 25 to 35 Hz, corresponding to the highest frequency of about 35 Hz. Related studies have shown [18] that soil parameters can be known in this study object elastic modulus of 78.7 MPa, the initial density of the roadbed is 1330 kg/m^3, substituted in Eq (3) can be calculated to obtain the roadbed soil shear modulus. The shear modulus of the roadbed is calculated to be 30.3 MPa. The vibration wave speed during the vibration compaction of the roadbed can be calculated according to Eq (4) [19]. The vibration wave velocity during vibration compaction of the roadbed is calculated to be 150.9 m/s. The wavelength corresponding to the highest frequency can be calculated according to Eq (5). The wavelength of vibration wave during vibratory compaction is calculated to be λ = 4.31 m.

$$\Delta l \le \left(\frac{1}{8} - \frac{1}{10}\right)\lambda \tag{2}$$

$$\mathrm{G} \le \frac{E}{2(1+\mu)} \tag{3}$$

$$c_s \le \sqrt{\frac{G}{\rho}} \tag{4}$$

$$\lambda \le \frac{c_s}{f} \tag{5}$$

where, λ is the wavelength corresponding to the highest frequency. G is shear modulus (MPa); E is modulus of elasticity (MPa); μ is Poisson's ratio; c_s is vibration wave velocity (m/s); f is maximum frequency (Hz). The mesh size for the finite element numerical simulation is thus determined as:

$$\Delta l \leq (0.43\sim0.54)m$$

In this paper, taking the calculation efficiency and accuracy into account, the grid size is 0.02 m in the center area of load application and 0.4 m at the boundary, and the fine grid and coarse grid are connected by gradient grid, as shown in Figure 3.

2.1.4. Loading and modeling

For the loading, the common medium and large YZZT39 roller parameters were selected, as shown in Table 1. During the simulation, once to four times compaction were applied and data were extracted, respectively.

Table 1. Numerical simulation input parameter.

Total operating weight (kg)	Static load on front drum (kg)	Eccentric force (kN)	Excitation frequency (Hz)
19,500	19,500	850	22–28

2.1.5. Constitutive model and parameter selection

The ideal elastoplastic model uses the Mohr-Coulomb model extended by Abaqus software to reflect the plastic properties of the soil [20], and the plastic potential surface of the traditional Mohr-Coulomb model on the stress space is an equilateral unequal hexagonal cone, whose plastic flow direction on the prism is not unique, which may cause the non-convergence of the calculation results, while the extended Mohr-Coulomb Coulomb model has a hyperbolic plastic potential surface in the meridional plane (Figure 4) and a segmentally symmetric ellipse in the π-plane (Figure 5), with the corner points removed, i.e., this plastic potential surface is smooth and the plastic flow direction is unique everywhere.

For the constitutive relations of the soil model, two constitutive models, linear elastic as well as ideal elastoplastic, are considered in this paper in order to accommodate nonlinear analysis [21]. The ideal elastic-plastic model uses the Mohr-Coulomb model extended by ABAQUS software to reflect the plastic properties of the soil. The plastic potential surface of the traditional Mohr-Coulomb model in stress space is a hexagonal cone with unequal sides, and its plastic flow direction is not unique on the prism, which may cause the non-convergence of calculation results. In contrast, the extended Mohr-Coulomb model has a hyperbolic plastic potential surface in the meridional plane (Figure 4) and a segmentally symmetric ellipse in the π-plane (Figure 5), with the corner points removed, this plastic potential surface is smooth and the plastic flow direction is unique everywhere [22].

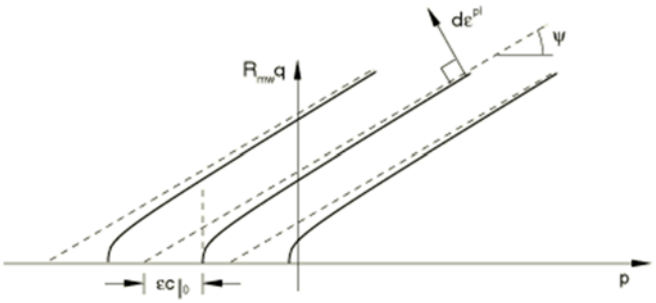

Figure 4. Projection of plastic potential surface on meridian plane.

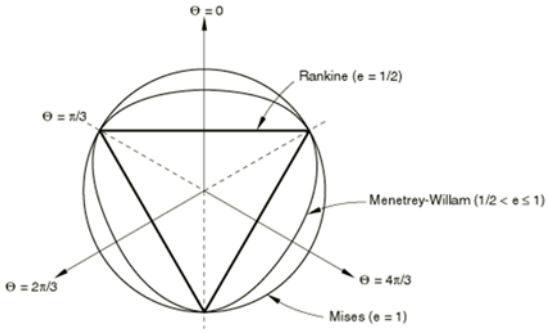

Figure 5. Intersection line between plastic potential surface and π plane.

2.2. Finite element secondary development

2.2.1. Establishing the relationship between "field" and roadbed strain

The following assumptions are made for the simulation model [23]:

- The strain in the horizontal and vertical directions during compaction of the roadbed is negligible compared to the model dimensions, and the model shape during compaction is considered rectangular;
- The roadbed is continuous, uniform and isotropic in the initial state and during compaction.
- Water will not seep during the calculation process.

The width of z-direction is set to 1 in the model and no deformation occurs, i.e., strain $\varepsilon_3 = 0$. The initial compaction degree K_0 is set to 80%. The calculation process and expression of the volume of the roadbed model during compaction, as shown in Eq (6). The real-time compaction degree K can be calculated by Eq (7). The density ρ and the maximum dry density ρ_{max} are calculated by Eq (8) as follows:

$$V_1 = xyz(1+\varepsilon_1)(1+\varepsilon_2)(1+\varepsilon_3) = V_0(1+\varepsilon_1)(1+\varepsilon_2) \tag{6}$$

$$K = \frac{\rho}{\rho_{max}} \tag{7}$$

$$\rho = \frac{m}{V}, \rho_{max} = \frac{m}{V_{min}} \tag{8}$$

where: x is the length of the model (m), the length of the model in this paper is 10 m; y is the thickness

of the layer to be compacted by the model (m), the thickness of the layer to be compacted in this paper is 0.3 m; z is the model width (m), since the model is a two-dimensional model, z = 1 m; ε_1 is strain in x-direction; ε_2 is strain in y-direction; ε_3 is strain in z-direction, $\varepsilon_3 = 0$; V_0 is initial volume of the model; K—real time compaction degree; ρ is density (kg/m^3) under the real time compaction degree corresponding to K; ρ_{max} is the maximum dry density (kg/m^3); m is weight (kg) corresponding to density ρ; V is volume (m^3) corresponding to density ρ; V_{min} is the volume corresponding to the maximum dry density ρ_{max} (m^3). During compaction, the weight of soil m is constant, the maximum dry density ρ_{max} of the soil is unchanged, the V_{min} corresponding to the maximum dry density ρ_{max} is unchanged, and only V and ρ change in real time. Combining Eqs (6)–(8), Equation (9) can be obtained. From the initial setting of compaction ρ_1 as 80%, the final relationship between real-time compaction degree K and strain can be obtained by substituting Eq (9) as shown in Eq (10). At this point, the relationship between the real-time compaction degree K and strain ε is determined by mathematical modeling.

$$K = \frac{V_{min}}{V_0(1+\varepsilon_1)(1+\varepsilon_2)} \tag{9}$$

$$K = \frac{0.8}{(1+\varepsilon_1)(1+\varepsilon_2)} \tag{10}$$

2.2.2. Establishing the relationship between “field” and shear strength of roadbed

Table 2. Shear strength of loess.

Moisture content (%)	Compaction degree (%)	Cohesive force (kPa)	Friction angle (°)
10.3	85	104.55	26.6
	90	142.42	28.8
	93	155.64	29.4
	95	173.79	32.8
11.3	85	74.12	23.6
	90	87.23	24.1
	93	134.1	29.4
	95	110.44	31.3
12.3	85	70.65	21.8
	90	73.89	22.1
	93	107.14	23.3
	95	101.59	24.8
14.3	85	39.92	19.8
	90	61.10	19.7
	93	64.09	23.4
	95	68.30	20.6

Based on existing studies [18], the relationship between the shear strength indexes corresponding to different moisture contents and compaction degrees of loess can be obtained, as shown in Table 2. By fitting, the relationship between compaction degree and shear strength index

corresponding to 10.3%, 11.3%, 12.3% and 14.3% of moisture content were obtained by Eq (11). The set initial compaction degree K_0 is 80% and the maximum compaction degree K_{max} is 100%. By fitting the equation and taking 2% as the step size, the "field" real-time compaction degree K can be generated to correspond to the soil shear strength as shown in Table 3. The data in Table 3 can be added to the Abaqus finite element numerical simulation to achieve real-time changes in the shear strength of the roadbed with compaction in the numerical simulation, thus improving the accuracy of the numerical simulation.

Table 3. The "field" compaction degree K corresponds to the shear strength of soil.

Compaction degree/K (%)	Moisture content ω = 10.3%		Moisture content ω = 11.3%		Moisture content ω = 12.3%		Moisture content ω = 14.3%	
	Cohesive force c (kPa)	Friction angle φ (°)	Cohesive force c (kPa)	Friction angle φ (°)	Cohesive force c (kPa)	Friction angle φ (°)	Cohesive force c (kPa)	Friction angle φ (°)
80	72.0	23.5	48.3	20.2	28.2	18.7	48.5	18.5
82	85.4	24.6	55.7	20.7	33.8	19.1	58.4	20.1
84	98.8	25.7	63.2	21.3	39.4	19.5	68.2	21.7
86	112.2	26.8	70.6	21.9	45.0	19.9	78.1	23.3
88	125.7	27.8	78.0	22.4	50.7	20.4	87.9	24.9
90	139.1	28.9	85.5	23.0	56.3	20.8	97.8	26.5
92	152.5	30.0	92.9	23.5	61.9	21.2	107.6	28.1
94	165.9	31.1	100.4	24.1	67.5	21.6	117.5	29.7
96	179.4	32.2	107.8	24.7	73.1	22.0	127.3	31.3
98	192.8	33.3	115.3	25.2	78.7	22.4	137.2	32.9
100	206.2	34.4	122.7	25.8	84.3	22.8	147.0	34.5

$$\begin{cases} c = 671.1K - 464.9 \\ \varphi = 54.6K - 20.2 \end{cases} \omega = 10.3\%$$
$$\begin{cases} c = 372.1K - 249.4 \\ \varphi = 28.2K - 2.4 \end{cases} \omega = 11.3\%$$
$$\begin{cases} c = 280.4K - 196.1 \\ \varphi = 20.4K + 2.4 \end{cases} \omega = 12.3\% \quad (11)$$
$$\begin{cases} c = 492.5K - 345.5 \\ \varphi = 80.0K - 45.5 \end{cases} \omega = 14.3\%$$

2.3. Intelligent compaction index

CMV is easy to calculate and it is relatively accurate. Therefore, it is now widely used as an intelligent compaction index [24]. When the intelligent roller compacts the roadbed at a certain rolling speed, its vibrating wheel generates an excitation force under the action of the continuous rotation of the eccentric block. The excitation force and the weight of the roller act together on the roadbed, making the compacted soil from a static state to a vibrating state. The soil also gradually becomes dense from loose, in this process, the compaction quality and stiffness of the soil will be improved with the compaction. The calculation method of CMV is shown in Eq (12).

$$CMV = C\frac{A_{2\omega}}{A_{\omega}} \tag{12}$$

where: A_{Ω} is fundamental corresponding to the amplitudes. $A_{2\Omega}$ is second harmonic corresponding amplitude. C is the constant, and 100 is employed in this paper.

In the initial stage of compaction, the soil is in a relatively loose state, and the compaction quality and stiffness are small. Therefore, the resistance of the soil to the vibrating wheel is also relatively small, as shown in Figure 6(a). As compaction proceeds, the compaction quality and stiffness of the soil increases, and the accompanying reaction force of the roadbed on the vibrating wheel also gradually increases, as shown in Figure 6(b).

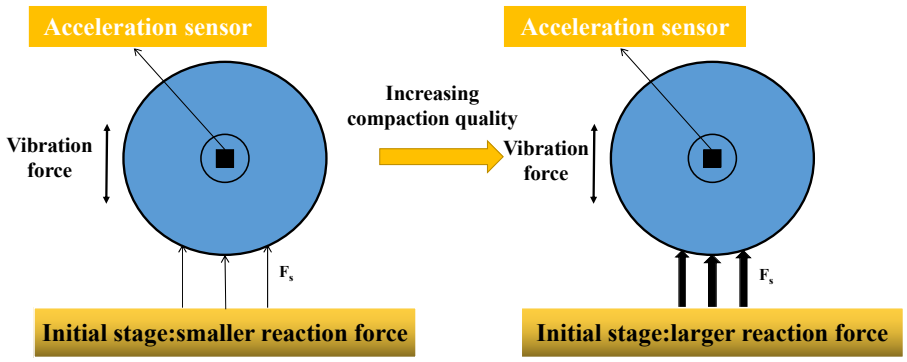

Figure 6. (a) The interaction between the vibration wheel and soil in the initial stage; (b) The interaction between vibration wheel and soil during compaction.

Studies have shown [25] that the stiffness of the roadbed is closely related to the vertical acceleration signal of the vibrating wheel. In the initial stage of compaction, the soil is in a relatively loose state, and the compaction quality and stiffness are small. Therefore, the resistance of the soil to the vibrating wheel is also relatively small, as shown in Figure 6(a). As compaction proceeds, the compaction quality and stiffness of the soil increases, and the accompanying reaction force of the roadbed on the vibrating wheel also gradually increases, as shown in Figure 6(b).

In the initial stage of compaction, because the resistance of the soil to the vibrating wheel is small and the eccentric block of the vibrating wheel is in the initial position (phase angle is 0), the excitation force generated by the vibrating wheel is a standard sinusoidal function, and the acceleration signal of the vibrating wheel collected is also a sinusoidal function, as shown in Figure 7(a). When the roadbed is in this stage of compaction process, with the increase of the resistance of the roadbed, the vibration wheel acceleration signal is no longer a single sinusoidal function, but a complex signal composed of multiple sinusoidal functions, due to the superposition of multiple sinusoidal functions, the amplitude also increases accordingly, as shown in Figure 7(b).

In the initial stage of compaction, the acceleration time domain signal of the vibrating wheel is a single sinusoidal function, and the acceleration frequency domain signal is obtained after the discrete Fourier transform, with only the amplitude of the first harmonic (fundamental), as shown in Figure 8(a). Additionally, as the compaction proceeds, the frequency domain signal of acceleration of the vibrating wheel appears as the second harmonic, as shown in Figure 8(b). At this time, the current compaction state is judged by the relationship between the ratio of the second harmonic to the amplitude of the primary harmonic.

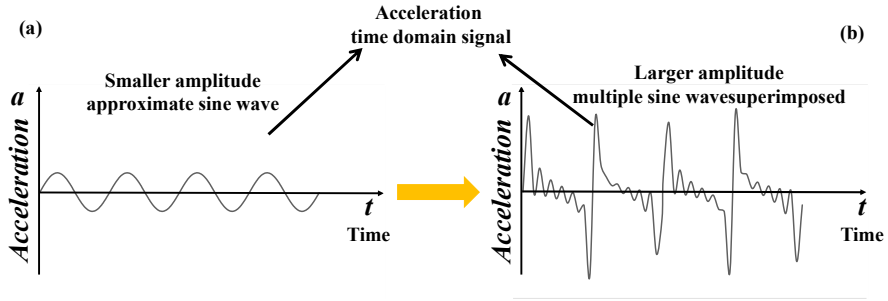

Figure 7. (a) Initial vibration wheel acceleration time domain signal; (b) Time domain signal of acceleration of vibrating wheel during compaction.

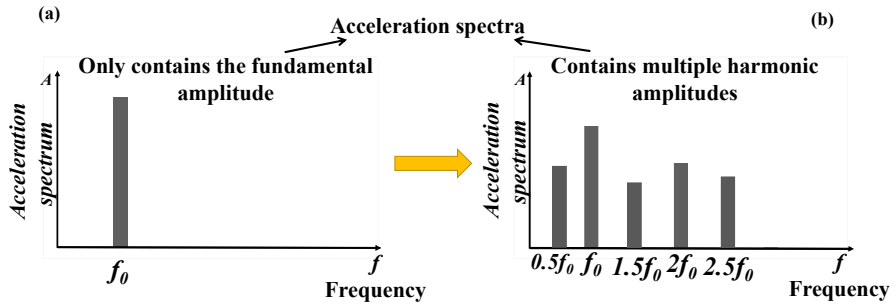

Figure 8. (a) Frequency domain signal of acceleration of vibration wheel in initial stage; (b) Frequency domain signal of acceleration of vibration wheel during compaction.

3. Results and discussion

3.1. Dynamics response analysis

Through the established numerical simulation model of the intelligent compaction process of the roadbed, the dynamic response of the roadbed during compaction, including the vertical displacement and vertical acceleration can be obtained, as shown in Figure 9. From Figure 9, it can be seen that: 1) the vertical displacement mainly occurs in the static compaction stage. In the first 0.5 s of contact between the vibration wheel and the roadbed, the vertical displacement changes sharply. In the subsequent compaction process, the growth of vertical displacement is smaller. 2) When the water content is 14.3%, the amplitude of vertical displacement curve is much larger than the amplitude of vertical displacement corresponding to other water contents. This is because the vertical displacement can reflect the soil compaction quality, when the soil compaction quality is larger, the vertical displacement under the same load is smaller, and vice versa. The moisture content of 14.3% is much larger than the optimal moisture content of 11.3%, which corresponds to the shear strength of the roadbed is less than the shear strength of the roadbed under other moisture content. At this time, the ability of the roadbed to resist deformation is reduced, when the same load acts on the roadbed, there is a sharp increase in the amplitude of the vertical position. 3) The amplitude of vertical acceleration is almost not affected by the water content. Comparing the vertical displacement under different water content, when the water content is 14.3%, the amplitude of vertical displacement changes sharply, and the amplitude of vertical acceleration does not show significant difference.

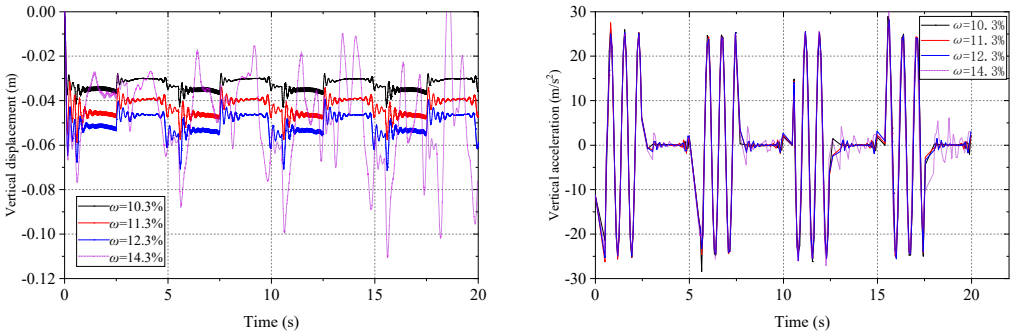

Figure 9. (a) Vertical displacement curve with time; (b) Vertical acceleration curve with time.

3.2. Correlation analysis of compaction degree and intelligent compaction index

The vertical displacement change of the roadbed in the compaction process can be calculated to obtain the compaction degree by the initial compaction degree K_0. The process of calculating compaction degree by vertical displacement is as follows: set the initial roadbed compaction degree as K_0, the thickness of roadbed loosened as U, the maximum roadbed compaction degree as $K_{max} = 1$, in the theoretical maximum vertical displacement x_{max} as shown in Eq (13), the theoretical maximum vertical displacement x_{max} corresponds to the compaction degree growth space as (1-K_0). In the compaction growth space, the relationship between the current vertical displacement x and compaction degree can be established, as shown in Eq (14). In this paper, the initial compaction degree $K_0 = 0.8$, and the thickness U of the top layer of the roadbed is 0.3 m. The real-time compaction degree and the vertical displacement can be calculated from (15) as follows:

$$x_{max} = U(1 - K_0) \tag{13}$$

$$K = K_0 + (1 - K_0)\frac{x}{U(1-K_0)} = K_0 + \frac{x}{U} \tag{14}$$

$$K = 0.8 + \frac{x}{0.3} \tag{15}$$

where, x is vertical displacement (m).

When the water content is 14.3%, the resistance to deformation of the roadbed decreases, and the law of vertical displacement amplitude during compaction is not obvious, so if the correlation is established with the intelligent compaction index, the wrong results will be obtained. Therefore, this paper selects the vertical displacement corresponding to water content of 10.3%, 11.3% and 12.3% to calculate the compaction degree, and the obtained compaction degree is shown in Figure 10.

From Figure 10, it can be seen that: 1) the roadbed with high shear strength is more difficult to be compacted. As the moisture content increased from 10.3% to 12.3%, the shear strength of the roadbed also increased. After the roadbed experienced four compaction passes, the compaction degree of the roadbed with water content of 10.3% increased the least. This is because the higher the shear strength of the soil, the more difficult it is to be compacted. In the same time, the compaction degree increase becomes smaller under the same excitation force. 2) Soil with the moisture content of 12.3% showed a compaction degree of more than 100% during compaction. At the beginning of each vibratory compaction pass, as the vibratory wheel starts the moment of vibration contact with the roadbed, in

addition to the excitation force, there is also an impact load, which is known from the structural dynamics [26], and the value of the impact load is double of the static load. When the excitation force and impact load act together on the roadbed, while the roadbed with a moisture content of 12.3% has a low resistance to deformation, so the compaction degree exceeds 100%.

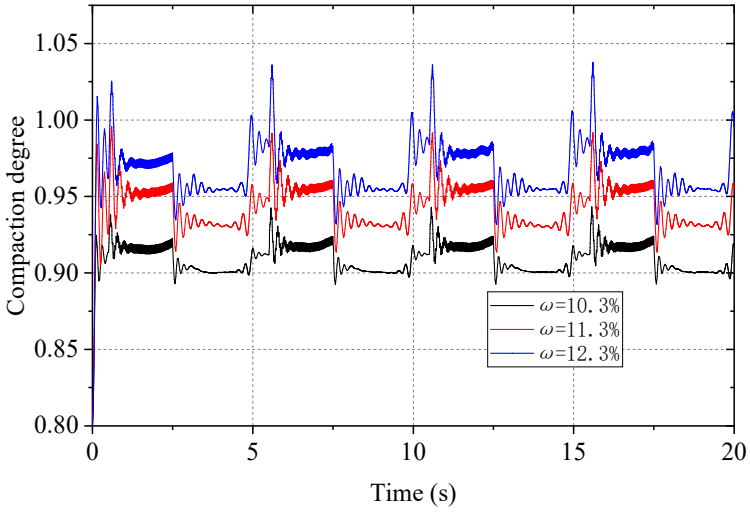

Figure 10. Compaction degree curve.

Table 4. The results of compaction degree and CMV.

	Moisture content ω = 10.3%	Moisture content ω = 11.3%	Moisture content ω = 12.3%
Compaction pass n = 1	91.68% / 9.87	95.34% / 12.24	97.41% / 13.45
Compaction pass n = 2	91.86% / 10.02	95.65% / 12.87	98.13% / 14.51
Compaction pass n = 3	91.87% / 9.89	95.66% / 12.39	98.16% / 14.66
Compaction pass n = 4	91.87% / 9.76	95.66% / 12.56	98.17% / 14.53

The compaction degree of the same vibration compaction process is averaged as the compaction degree of the current compaction pass, and the acceleration signal of each vibration compaction process is discrete Fourier transformed to calculate the CMV, and CMV of the current compaction pass is obtained. The calculation results of compaction degree and CMV are obtained as shown in Table 4. Based on Table 4, the relationship between compaction degree and CMV is obtained as shown in Figure 11. From Figure 11, it can be seen: 1) the main stage of the increase in the compaction quality of the roadbed is before the end of the first compaction. At the end of the first compaction, the compaction of the roadbed increased rapidly from the initial compaction of 80% and stabilized to 91.68%, 95.34% and 97.41%, respectively. CMV also increased from 0 at the beginning of compaction to 9.87, 11.24 and 13.45. 2) After the end of the first compaction, the influence of compaction passes on the compaction degree and CMV is small. Since the second rolling, the compaction degree and CMV of the roadbed tend to level off and almost stop increasing. 3) The compaction degree has a good positive correlation with CMV. From the fitted relationship between compaction degree and CMV, it is known that their correlation coefficient $R^2 > 0.9$, which indicates that CMV has a good correlation with compaction, so CMV index can be used for continuous testing

of intelligent compaction quality.

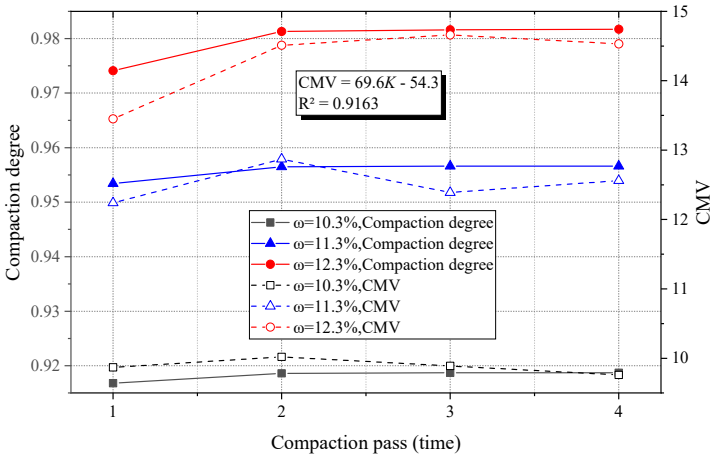

Figure 11. Curve between compactness and CMV.

3.3. Analysis of the effect of moisture content on intelligent compaction index

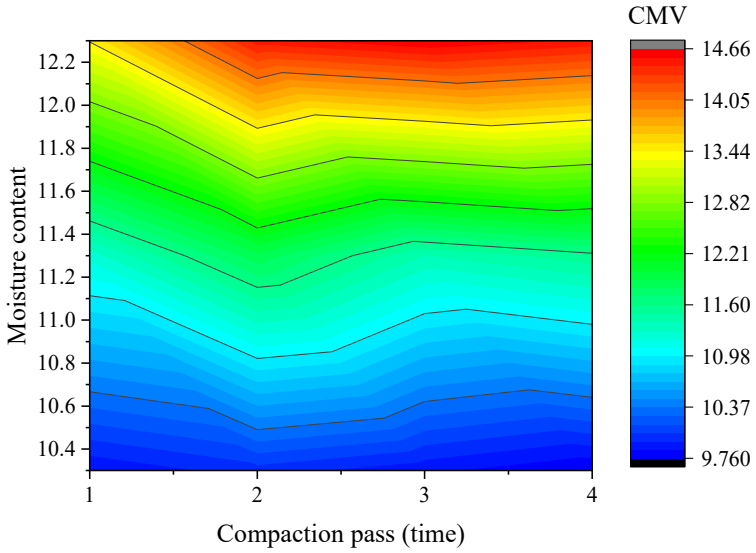

Figure 12. Cloud diagram of the relationship between moisture content and compaction pass and CMV.

In each compaction pass, the acceleration signals of roadbed with different water content are subjected to discrete Fourier transform to calculate the CMV, and the CMV corresponding to the current water content and compaction pass is obtained. In turn, the relationship between water content and number of compaction passes and CMV is obtained, as shown in Figure 12. From Figure 12, it can be seen that: 1) the CMV gradually increases with the increase of water content. This is because as the water content increases, the shear strength of the soil decreases, the resistance to deformation decreases, and the deformation under the same load increases, bringing about an increase in the growth of

compaction degree. 2) At the end of the second compaction, CMV increased slightly compared with that at the end of the first compaction and stabilized at the end of the second compaction. 3) From the perspective of improving the compaction quality of the roadbed, the water content of the roadbed should be considered to be set slightly higher than the optimal water content of the roadbed. When the moisture content of the roadbed is about 1% greater than the optimal moisture content, the compaction quality of the roadbed grows fastest and the compaction effect is better. If the moisture content of the roadbed is less than the optimal moisture content, the roadbed is difficult to be compacted; if the moisture content of the roadbed is greater than the optimal moisture content of more than 1%, the roadbed in the compaction process there is the possibility of damage.

4. Conclusions

In this paper, through the secondary development of Abaqus finite element numerical simulation software, the refined simulation model is constructed to design the numerical simulation conditions of roadbed compaction under different water content. The correlation between compaction degree and intelligent compaction index CMV is established, and the correlation between water content and CMV is analyzed. The conclusions obtained in this paper are as follows:

- The vertical displacement mainly occurs in the static compaction stage. The vertical displacement changes sharply in the first 0.5s when the vibrating wheel is in contact with the roadbed. In the subsequent compaction process, the growth of vertical displacement is smaller. When the moisture content is 14.3%, the amplitude of the vertical displacement curve is much larger than the amplitude of vertical displacement corresponding to other moisture contents.
- The amplitude of vertical acceleration is almost not affected by the water content. Comparing the vertical displacement under different water contents, when the water content is 14.3%, the amplitude of vertical displacement changes sharply and the amplitude of vertical acceleration does not show a significant difference.
- The main stage of the increase in the compaction quality of the roadbed is before the end of the first compaction. At the end of the first rolling, the compaction degree of the roadbed increases rapidly from 80% to 91.68%, 95.34% and 97.41%, respectively. CMV also increases from 0 at the beginning of compaction to 9.87, 11.24 and 13.45. After the end of the first rolling, the influence of rolling passes on the compaction and CMV is small. From the beginning of the second rolling, the compaction degree and CMV of the roadbed level off and almost stop increasing.
- With the increase of water content, CMV gradually increases. At the end of the second compaction, CMV increases slightly compared with that at the end of the first compaction and stabilizes at the end of the second compaction. In addition, from the perspective of improving the compaction quality of the roadbed, the water content of the roadbed should be considered to be set slightly higher than the optimal water content of the roadbed by about 1% within the assumptions of this paper.

Use of AI tools declaration

The authors declare they have not used Artificial Intelligence (AI) tools in the creation of this article.

Acknowledgments

This research was funded by National Key Research and Development Project of China (No. 2020YFB1600102).

Conflict of interest

We declare that there are no conflicts of interest.

References

1. Y. Ma, F. Chen, T. Ma, X. M. Huang, Y. Zhang, Intelligent compaction: An improved quality monitoring and control of asphalt pavement construction technology, *IEEE Trans. Intell. Transp. Syst.*, **23** (2022), 14875–14882. https://doi.org/10.1109/TITS.2021.3134699
2. Y. Ma, Y. Zhang, W. Zhao, X. M. Ding, Z. W. Wang, T. Ma, Assessment of intelligent compaction quality evaluation index and uniformity, *J. Transp. Eng. Part B. Pavements*, **148** (2022). https://doi.org/10.1061/JPEODX.00003
3. J. S. Qian, H. L. Wang, P. Wang, Test and control methods for on-site compaction of fine sand subgrade on coastal regions, in *New Frontiers in Engineering Geology and the Environment*, Springer, (2013), 75–78. https://doi.org/10.1007/978-3-642-31671-5_11
4. F. Wang, H. Li, A nonparametric approach for characterizing soil spatial variability based on cone penetration test data, *Bull. Eng. Geol. Environ.*, **80** (2021), 1073–1089. https://doi.org/10.1007/s10064-020-01976-8
5. Editorial Department of China Journal of Highway and Transport, Review on China's pavement engineering research·2020, *China J. Highway Transp.*, **33** (2020), 1–66.
6. R. Anderegg, K. Kaufmann, Intelligent compaction with vibratory rollers: Feedback control systems in automatic compaction and compaction control, *Transp. Res. Rec. J. Transp. Research Board*, **1868** (2004), 124–134. https://doi.org/10.3141/1868-13
7. X. Y. Jia, W. Hu, P. Polaczyk, H. R. Gong, B. S. Huang, Comparative evaluation of compacting process for base materials using lab compaction methods, *Transp. Res. Rec.*, **2673** (2019), 558–567. https://doi.org/10.1177/03611981198379
8. T. Jia, T. J. He, Z. D. Qian, Y. Li, Research of continuous compaction detection method based on embedded system, in *COTA International Conference of Transportation Professionals*, 2019. https://doi.org/10.1061/9780784482292.065
9. Q. Zhang, Z. An, Z. Huangfu, Q. Li, A review on roller compaction quality control and assurance methods for earthwork in five application scenarios, *Materials*, **15** (2022), 2610. https://doi.org/10.3390/ma15072610
10. W. Hu, X. Shu, X. Y. Jia, B. S. Huang, Recommendations on intelligent compaction parameters for asphalt resurfacing quality evaluation, *J. Constr. Eng. Manage.*, **143** (2017). https://doi.org/10.1061/(ASCE)CO.1943-7862.0001361
11. Q. W. Xu, G. K. Chang, Evaluation of intelligent compaction for asphalt materials, *Autom. Constr.*, **30** (2013), 104–112. https://doi.org/10.1016/j.autcon.2012.11.015

12. Y. Ma, Y. C. Luan, W. G. Zhang, Y. Q. Zhang, Numerical simulation of intelligent compaction for subgrade construction, *J. Cent. South Univ.*, **27** (2020), 2173–2184. https://doi.org/10.1007/s11771-020-4439-2
13. Y. Ma, F. Zhou, H. Tao, Dynamic simulation and evolution of key control parameters for intelligent compaction of subgrade, *J. Cent. South Univ. (Sci. Technol.)*, **52** (2021), 2246–2257. https://doi.org/10.11817/j.issn.1672-7207.2021.07.012
14. A. Haider, E. X. Song, P. Li, Numerical simulation and absorbing boundary conditions for wave propagation in a semi-infinite media with a linear isotropic hardening plastic model, *Soil Dyn. Earthquake Eng.*, **125** (2019), 105627. https://doi.org/10.1016/j.soildyn.2019.04.001
15. A. J. Deeks, M. F. Randolph, Axisymmetrical time-domain transmitting boundaries, *J. Eng. Mech.-ASCE*, **120** (1994), 25–42. https://doi.org/10.1061/(ASCE)0733-9399(1994)120:1(25)
16. X. Zhao, *Study on Intelligent Compaction Control Technology of Subgrade*, PhD thesis, Chang'an University, 2016.
17. X. Teng, *Numerical Analysis and Quality Control of Dynamic Consolidation of Silty Soil Subgrade in Yellow River Alluvial Plain*, M.S. thesis, Shandong University, 2017.
18. K. Chen, *Study on Strength and Deformation of Compacted Loess and Its Microstructure for Highway Engineering*, PhD thesis, Chang'an University, 2016.
19. Y. Chen, D. Xu, *FLAC/FLAC3D Fundamental and Engineering Examples*, China Water Conservancy and Hydropower Publishing House, 2009.
20. Z. An, T. Liu, Q. Zhang, Z. Zhang, Z. Huangfu, Q. Li, Vibration compaction process model for rockfill materials considering viscoelastic-plastic deformation, *Autom. Constr.*, **131** (2021), 103889. https://doi.org/10.1016/j.autcon.2021.103889
21. Y. Ma, H. Liang, Y. X. You, W. G. Zhang, L. M. Guo, J. W. Fan, et al., Elastic-viscoplastic constitutive model of soil under cyclic loading, *Adv. Civ. Eng.*, **2021** (2021). https://doi.org/10.1155/2021/1602431
22. L. Mi, The influence of base modulus on compaction energy in subgrade, *J. China Railway Soc.*, **6** (2008), 69–74. https://doi.org/10.3321/j.issn:1001-8360.2008.06.013
23. W. Hu, X. Y. Jia, X. Y. Zhu, A. W. Su, Y. Du, B. S. Huang, Influence of moisture content on intelligent soil compaction, *Autom. Constr.*, **113** (2020), 103141. https://doi.org/10.1016/j.autcon.2020.103141
24. Z. An, T. Liu, Z. Huangfu, Q. Zhang, C. Li, Q. Li, Neural network model for evaluating compaction quality of rockfill materials by compaction meter value, *J. Hydroelectr. Eng.*, **39** (2020), 110–120.
25. H. C. Dan, D. Yang, X. Liu, A. P. Peng, Z. Zhang, Experimental investigation on dynamic response of asphalt pavement using SmartRock sensor under vibrating compaction loading, *Constr. Build. Mater.*, **247** (2020), 118592. https://doi.org/10.1016/j.conbuildmat.2020.118592
26. Y. Long, *Structural Mechanics*, Higher Education Press, 2001.

AIMS Press